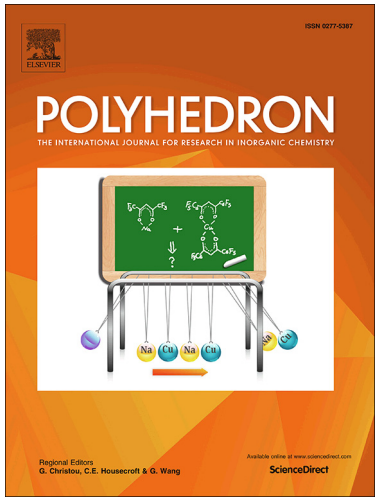

Preparation, Thermal Analyses and Biological Activities of Co (II) and Cr (III) Complexes with 2-Acetylpyridine-6-Bromo-2-Naphthoyl Acylhydrazone

Xin-jie Zong, Xiang-rong Liu, Shun-sheng Zhao, Zai-wen Yang

PII: S0277-5387(19)30397-3
DOI: https://doi.org/10.1016/j.poly.2019.05.059
Reference: POLY 13984

To appear in: *Polyhedron*

Received Date: 20 January 2019
Revised Date: 24 May 2019
Accepted Date: 29 May 2019

Please cite this article as: X-j. Zong, X-r. Liu, S-s. Zhao, Z-w. Yang, Preparation, Thermal Analyses and Biological Activities of Co (II) and Cr (III) Complexes with 2-Acetylpyridine-6-Bromo-2-Naphthoyl Acylhydrazone, *Polyhedron* (2019), doi: https://doi.org/10.1016/j.poly.2019.05.059

Preparation, Thermal Analyses and Biological Activities of Co (II) and Cr (III) Complexes with 2-Acetylpyridine-6-Bromo-2-Naphthoyl Acylhydrazone

Xin-jie Zong[a], Xiang-rong Liu[a,]*, Shun-sheng Zhao[a], Zai-wen Yang[a]

[a]*College of Chemistry and Chemical Engineering*, *Xi'an University of Science and Technology*, *Xi'an 710054*, *China*

*Corresponding author. E-mail address: liuxiangrongxk@163.com.

ABSTRACT

Novel six-coordinated octahedral Co(II) complex [$C_{36}H_{26}Br_2CoN_7O_5$, **1**] and Cr(III) complex [$C_{36}H_{26}Br_2CrN_6O_2$, **2**] were prepared by the chelation reaction of the ligand 4-methoxybenzaldehyde-6-bromo-2-naphthoyl acylhydrazone and 2-acetylpyridine with $Co(NO_3)_2 \cdot 6H_2O$ or $CrCl_3 \cdot 6H_2O$ in ethanol, and it is interesting that the coordination organic group wasn't the original acylhydrazone. Based on X-ray single crystal diffraction technique, the structures of **1** and **2** were characterized, which revealed **1** belonged to monoclinic system and $P2_1/n$ space group, whereas **2** belonged to triclinic system and *P*-1 space group. The apparent activation energies of the thermal decomposition of **1** and **2** showed **1** had far better thermal stability than **2**. Both of **1** and **2** quenched the intrinsic fluorescence of BSA through static processes, which suggested **1** and **2** could bind to BSA effectively and the non fluorescent ground state complexes were formed. UV-vis spectra indicated each complex bound to ct-DNA by an intercalative mode. Microcalorimetry experiments illustrated the interactions of two complexes with BSA and ct-DNA were both spontaneous endothermic processes and the binding activities of **1** with BSA and ct-DNA were greater than that of **2**. The minimum inhibitory concentrations(MIC) of each complex against *Escherichia coli*, *Staphylococcus aureus*, *Bacillus subtilis* and *Pseudomonas aeruginosa* were all 50 $\mu g \cdot mL^{-1}$.

***Keywords*:** Complex; Thermal stability; BSA; ct-DNA; Biological activity

1. Introduction

Acylhydrazone was a special Schiff base and the bioactive group (-CONHN=CH-) existed in its molecular structure, so it had wide application in fields of pesticide and medicine [1-6]. The existence of nitrogen and oxygen atoms in the bioactive group made it possess strong coordination abilities, and the existence of tautomer made it have

various coordination modes [7], especially acylhydrazone metal complexes, which can serve as drugs for antibacterial [8], antitumor [9], antiviral [10] and anticancer [11]. According to the reports [12,13], acylhydrazone Co(II) and Cr(III) complexes had certain better bioactivities. For example, C.Z. Zheng studied the inhibition activities of Ni(II) and Cr(III) complexes with 2-furaldehyde benzoylhydrazone against *Escherichia coli*, *Staphylococcus aureus* and *Pseudomonas aeruginosa* by oxford cup methods, which showed these complexes had certain inhibition activities against three kinds of bacteria [12]. R.S. Hunoor designed Co(II), Ni(II), Cu(II) and Zn(II) complexes with isatinyl-2-aminobenzoylhydrazone, and studied the vitro anticancer activities of these complexes against EAC cells, adenocarcinoma HT29, kidney cancer K293 and breast cancer MDA231 by MTT assay, they found Co(II) complex exhibited impressive activities with IC_{50} against EAC cells and HT29, was a potential anticancer drug [13].

Naphthalene was one of PAHs and compounds containing naphthalene rings also had strong bioactivities and were widely applied in pesticide and medicine [14-15]. In this paper, compounds containing naphthalene rings were introduced into the molecular structure of acylhydrazone to obtain novel acylhydrazone compounds and their metal complexes possessing biological activities of both groups.

Based on the above facts, this paper focused on the preparation of Co(II) and Cr(III) complexes with 2-acetylpyridine-6-bromo-2-naphthoyl acylhydrazone, which were characterized by elemental analyses and X-ray single crystal diffraction. The thermal decomposition behaviors of the complexes were analyzed by thermogravimetry. The interaction modes of the complexes with BSA and ct-DNA were studied by fluorescence spectrometry, UV-vis spectrometry and microcalorimetry. The inhibition activities of the complexes against four kinds of bacteria were studied by oxford cup method. Preparation routes of Co(II) complex(**1**)

and Cr(III) complex(**2**) were shown in Scheme 1.

Scheme 1

2. Experimental

2.1. Materials and methods

Hydrazine hydrate(80%), ethanol, methanol and DMF were obtained from Fuyu Fine Chemical Industry. 4-methoxybenzaldehyde, 2-acetylpyridine, cobalt nitrate hexahydrate, chromium chloride hexahydrate and BSA were attained from Bailingwei Co. Ltd.. Methyl 6-bromo-2-naphthoate and ct-DNA were bought from Bide Pharmatech Ltd. and Sigma Aldrich, respectively. *Escherichia coli*, *Staphylococcus aureus*, *Bacillus subtilis* and *Pseudomonas aeruginosa* were purchased from China Center of Industrial Culture Collection (CICC). All reagents and chemicals were purchased from commercial sources and used without purification.

Single crystal structures were recorded on Bruker Smart Apex II CCD X-ray single crystal diffractometer. Melting points were determined by WRS-2U melting point apparatus. Elemental compositions were performed on PE-2400-II elemental analyzer. Thermogravimetric data were obtained by TG-DSC1 HT thermogravimetric analyzer. UV-vis spectra were measured by TU-1950 UV spectrophotometer. Fluorescence spectra were carried out with LS 55 fluorescence spectrometer. Thermogenic curves were studied by C80 microcalorimeter.

*2.2. Preparation of **1** and **2***

2.2.1. Preparation of $[C_{19}H_{15}BrN_2O_2]$(precursor ligand)

6-bromo-2-naphthoyl acylhydrazine was synthesized as described previously [16]. A mixture of 4-methoxybenzaldehyde (6.1 μL, 0.05 mmol), 6-bromo-2-naphthoyl acylhydrazine (0.0133g, 0.05 mmol) and methanol (20 mL) was refluxed with stirring at 60 ℃ for 2 h. Transparent acicular crystal could be obtained after about 2 days. Yield:

73%. m.p.: 230~231 ℃. Found for $C_{19}H_{15}BrN_2O_2$(383.24 g·mol^{-1}): C, 59.67; H, 4.03; N,7.36. Calcd: C, 59.55, H, 3.95; N, 7.31.

*2.2.2. Preparation of [$C_{36}H_{26}Br_2CoN_7O_5$](**1**) and [$C_{36}H_{26}Br_2CrN_6O_2$](**2**)*

A mixture of precursor ligand (0.0383g, 0.1 mmol), 2-acetylpyridine (6 drops) and absolute ethanol (20 mL) was refluxed at 60 ℃ for 5 min, and then ethanol solution(5 mL) containing $Co(NO_3)_2·6H_2O$ (0.0146 g, 0.05 mmol) was added to the mixture for refluxing at 73 ℃ for 6 h with stirring. Red-brown transparent acicular crystal **1** could be obtained about 10 days. Yield: 73%. m.p.: 267~268 ℃. Found for $C_{36}H_{26}Br_2CoN_7O_5$(855.46 g·mol^{-1}): C, 50.29; H, 3.26; N, 11.61. Calcd: C, 50.50; H, 3.04; N, 11.46.

Complex **2** was obtained as reddish black transparent acicular crystal in a manner similar to that used to obtain **1**, except using $CrCl_3·6H_2O$ instead of $Co(NO_3)_2·6H_2O$, and the reaction time was 9 h. Yield: 86%. m.p.: 227~228 ℃. Found for $C_{36}H_{26}Br_2CrN_6O_2$(788.46 g·mol^{-1}): C, 55.21; H, 3.47; N, 10.43. Calcd: C, 54.79; H, 3.30; N, 10.65.

In order to explore the preparation mechanism of two complexes, two preparation routes were designed in Scheme 2.

Scheme 2

As seen from Scheme 2, the new ligands in two complexes can't be prepared in the case of single or mixed solvents by the above two methods. So we infered the preparation mechanisms of two complexes, which were shown in Scheme 3. In Scheme 3, precursor ligand was firstly hydrolyzed in the presence of acids (Hydrolysis of metal ions caused the solution to be weak acidic) and ethanol (step ①), and 6-bromo-2-naphtholy acylhydrazine was formed [17]. Then, the new ligands in two complexes were obtained in the order of nucleophilic addition reaction(step ②), rearrangement

reaction(step ③), and elimination reaction(step ④). Finally, two complexes were prepared by the chelation reaction of new ligand and metal ions (Co(II) and Cr(III)) (step ⑤).

Scheme 3

2.3. X-ray structure determination and refinement

The X-ray diffraction measurements of **1** and **2** were collected on Bruker Smart Apex II CCD diffractometer with *ω/2θ* and Mo Kα radiation (*λ*=0.71073 Å) at 296(2) K. The structures of **1** and **2** were solved by direct methods, which yielded the positions of all non-hydrogen atoms, and then isotropical and anisotropical parameters of them were refined using full-matrix least square method based on SHELX-97 Program [18].

2.4. Thermal stability experiments

The thermal decomposition processes of **1** and **2** were studied at heating rates of 5, 10 and 15 ℃·min^{-1} from room temperature to 800 ℃ by thermogravimetric analyzer under nitrogen atmosphere.

2.5. BSA binding experiments

The BSA solution (1×10^{-7} mol·L^{-1}) was prepared by dissolving BSA solid in Tris-HCl buffer solution (0.01 mol·L^{-1}, pH 7.2, 50 mL). Each complex solution (1×10^{-5} mol·L^{-1}) was obtained by a mixture of DMF and Tris-HCl buffer solution (v/v=5:95, 50 mL). The interactions of the complexes with BSA by fluorescence spectra were performed keeping fixed BSA concentration while varying the complex concentration. Each fluorescence curve was recorded every 2 min. The excitation wavelength was 280 nm.

2.6. ct-DNA binding experiments

The Tris-HCl buffer solution was obtained in a manner similar to that used in BSA binding experiments, except that the pH was 7.9. ct-DNA solution was prepared and its

absorbance ratio A_{260}/A_{280} was considered to be up to standard for purity between 1.8 and 1.9. According to the conversion formula of DNA concentration : $C_{DNA}=A_{260}/6600$ $L \cdot mol^{-1} \cdot cm^{-1}$, the concentration of ct-DNA solution was 2.88×10^{-4} $mol \cdot L^{-1}$ [19]. Each complex solution(1×10^{-5} $mol \cdot L^{-1}$) was obtained by a mixture of DMF and Tris-HCl buffer solution(v/v=5:95, 50 mL). The interactions of the complexes with ct-DNA were performed keeping fixed complex concentration while varying the DNA concentration using UV-vis spectra. Each UV-vis spectra was recorded every 5 min. The scanning wavelength range was 250~500 nm.

2.7. Microcalorimetry experiments

The thermogenic curves of the interactions of each complex with BSA and ct-DNA were investigated by C80 microcalorimetry at 28 ℃. BSA and ct-DNA solutions used in the experiment were the same as that used in BSA and ct-DNA binding experiments. Firstly, the Tris-HCl buffer solution (1 mL) and each complex solution (1 mL) were added into the bottom of reference and sample cell, respectively, and then ct-DNA/BSA solution(1 mL) was added into the upper of two cells. The solutions in upper and bottom cells were mixed when the fluctuation of the heat flow was small.

2.8. Antibacterial experiments

Four kinds of bacteria namely *Escherichia coli*, *Staphylococcus aureus*, *Bacillus subtilis* and *Pseudomonas aeruginosa* were used to screen the antibacterial activities of **1** and **2**, which were inoculated at least 3 times. Each complex was dissolved in DMF to a final concentration of 200 $\mu g \cdot mL^{-1}$. In order to determine the minimum inhibitory concentration of **1** and **2**, both of **1** and **2** were diluted by double dilution method. DMF was considered as blank control and gentamycin sulfate was as control drug. Based on oxford cup method, the antibacterial experiments were carried out in triplicate under strict aseptic conditions. The diameters (mm) of inhibition zone of the complexes were

larger than that of blank control showed the inhibition activities of complexes, which were expressed in terms of the average diameters of inhibition zone.

3. Results and discussion

3.1. Description of single crystal structures

Crystallographic data, selected bond length(Å) and angle(°) of **1** and **2** were shown in Tables 1 and 2, respectively. The molecular structures of **1** and **2** were illustrated in Figs.1 and 3, and crystal packing structures of **1** and **2** were displayed in Figs.2 and 4.

Tables 1-2

Figs.1-4

There was a Co(II) ion and two new ligands in the molecular structure of **1** in Fig.1, a six-coordinated octahedral structure centered on Co(II) ion was obtained by the coordination of two oxygen atoms, two imino nitrogen atoms and two pyridine nitrogen atoms with Co(II) ion. The bond angles of [N(2)-Co(1)-O(2)], [N(5)-Co(1)-N(3)] and [O(1)-Co(1)-O(2)] were 93.3(4)°, 97.9(4)° and 90.5(3)°, indicating the octahedral structure was distorted. The bond lengths of Co(1)-N(2), Co(1)-N(3), Co(1)-N(5), Co(1)-N(6), Co(1)-O(1) and Co(1)-O(2) were 1.849(9), 1.921(10), 1.865(9), 1.953(11), 1.907(7) and 1.902(8) Å, which were comparable to the similar complexes [20]. It can be seen that the bond lengths of Co(1)-N(2) and Co(1)-N(5) were shorter than that of Co(1)-O(1) and Co(1)-O(2), and the bond lengths of Co(1)-O(1) and Co(1)-O(2) were shorter than that of Co(1)-N(3) and Co(1)-N(6), indicating nitrogen atoms had better coordination abilities than oxygen atoms in the bioactive group, oxygen atoms had better coordination abilities than pyridine nitrogen atoms. The O(1)-C(11)(1.330(13) Å) was a typical C-O single bond, and N(2)-C(12)(1.277 Å) was shorter than N(1)-C(11)(1.313 Å), showing **1** existed in form of enols after coordination [21,22]. As seen from Fig.2, there were π-π stacking interactions between naphthalene rings and pyridine

rings (J-type stacking) in **1**, belonging to weak interactions, the π-π stacking interaction extended to a three dimensional network structure. The constitutes and structures of **2** were similar to **1**.

3.2. Thermal stability analyses

Figs.5 and 6 dispalyed the TG-DTG curves of **1** and **2** at heating rates of 5, 10 and 15 ℃·min^{-1}, respectively. There were two steps for the thermal decomposition of **1**. At the first stage, the mass loss at heating rate of 5 ℃·min^{-1} was 2.95% at 91.72~171.74 ℃, connected with the loss of water(Calcd: 2.34%). At the second stage, the mass losses at heating rates of 10 and 15 ℃·min^{-1} were great different from that of at heating rate of 5 ℃·min^{-1}, the mass losses at heating rates of 5, 10 and 15 ℃·min^{-1} were 71.57%, 55.14 and 53.83% from 225 to 800 ℃, it was inferred that the mass loss resulted from the complete fracture of naphthalene rings, pyridine rings and C-Br single bonds(Calcd: 73.32%), which was similar to the mass loss at heating rate of 5 ℃·min^{-1}, it was because the greater the heating rate was, the more serious the temperature hysteresis was. If the heating rate was too fast, the complexes didn't respond adequately and the weightless step would be inaccurate or unmeasured. After 800 ℃, the remaining amount of **1** was 25.48% at heating rate of 5 ℃·min^{-1}, it was inferred that the residue was tricobalt tetraoxide(Calcd: 24.34%). The thermal decomposition process of **2** was the same as that of **1**, the first stage at heating rates of 5, 10 and 15 ℃·min^{-1} with mass losses of 5.70%, 4.89% and 5.54% from 78.13 to 160.41 ℃ were assigned to the loss of water. The second decomposition stage with the mass losses of 54.22%, 46.27% and 45.70% at heating rates of 5, 10 and 15 ℃·min^{-1} was considered as the complete fracture of naphthalene rings, pyridine rings and C-Br single bonds(Calcd: 54.09%), which was similar to the mass loss at heating rate of

5 ℃·min^{-1}. At last, the remaining amount of **1** was 40.27% at heating rate of 5 ℃·min^{-1}, it was inferred the residue was chromium oxide (Calcd: 36.21%).

Figs.5-6

The apparent activation energy(E_a) of **1** and **2** at the second stage can be obtained by Kissinger [23] and Ozawa equation [24], the formulas were as follows.

$$\ln\left(\frac{\beta}{T_p^2}\right) = \ln\left(\frac{AR}{E_a}\right) - \frac{E_a}{RT_p} \qquad \text{Kissinger} \qquad (1)$$

$$\lg\beta = \lg\left[\frac{AE_a}{RG(\alpha)}\right] - 2.315 - 0.4567\frac{E_a}{RT_p} \qquad \text{Ozawa} \qquad (2)$$

Where E_a refers to the apparent activation energy, T_P is the maximum temperature of endothermic peak, β is the heating rate, A is the pre-exponential factor, R is the gas constant and $G(\alpha)$ is the integral mechanism function.

The results were shown in Table 3. As seen from Table 3, E_a(**1**) was more than twice as much as E_a(**2**), showing **1** was more stable than **2**, this was because the bond lengths of all coordination bonds of **1** were generally shorter than those of corresponding coordination bonds of **2**, so that the bond energies of all coordination bonds of **1** were higher than those of corresponding coordination bonds of **2**, so **1** needed to absorb more energies than **2** in the thermal decomposition processes.

Table 3

3.3. BSA binding studies

In virtue of the existences of amino acid residues in BSA, so BSA emits fluorescence when it is excited [25]. Fluorescence quenching is divided into static quenching and dynamic quenching, static quenching is caused by the formation of ground state complexes between quencher and BSA, while dynamic quenching results from colliding with each other. The abilitites of complexes to quench the fluorescence were related to the interactions between complexes and BSA, which could be described

by Stern-Volmer and Lineweaver-Burk equations [26,27], respectively. The formulas were as follows.

$$F_0 / F = K_{sv}[Q] + 1 = K_q \cdot \tau_0 [Q] + 1 \qquad \text{Stern-Volmer} \qquad (3)$$

$$\lg[(F_0 - F)/F] = n \lg[Q] + \lg K_A \qquad \text{Lineweaver-Burk} \qquad (4)$$

Where F_0/F refers to fluorescence intensity ratio before and after the addition of the quencher, Q is the concentration of complexes, $\tau_0(10^{-8}$ s) is the average lifetime of the biomolecule without quencher, K_{sv} is the Stern-Volmer quenching constant, K_q is the bimolecular quenching constant, n is binding site and K_A is the binding constant.

The fluorescence emission spectra of the interactions of **1** and **2** with BSA were shown in Figs.7 and 8 (Inset: Plots of F_0/F against Q of **1** and **2**). BSA solution showed strong fluorescence emission peak at 342 nm, and the fluorescence intensity slightly decreased and the emission peak occurred weak-blue shift with the increase of the concentration of **1** and **2**, illustrating each complex caused the changes of microenvironment and conformation for BSA.

Figs.7-8

Firstly, it was assumed that the interactions between two complexes and BSA were the dynamic quenching processes. According to the Stern-Volmer equation, K_{sv} and K_q for static quenching interaction were obtained from the plots of F_0/F and Q (as insets in Figs.7 and 8) and shown in Table 4. As seen from Table 4, both of K_q were larger than the maximum scatter collision quenching constant(2×10^{10} L·mol^{-1}·s^{-1}), indicating the non fluorescent ground state complexes were formed between each complex and BSA, corresponding to static quenching mechanism.

On the basis of Lineweaver-Burk equation, n and K_A were obtained from the plots of lg[(F_0-F)/F] against lg[Q] in Fig.9 and listed in Table 5. It can be seen from Table 5, the non fluorescent ground state complexes were formed through each complex with BSA in proportion to 1:1 [28], and K_A(**1**) was slightly larger than K_A(**2**), showing the

binding ability of **1** with BSA was greater than that of **2**.

Fig.9

Tables 4-5

3.4. DNA binding studies

Figs.10 and 11 displayed UV-vis spectra of the interaction of each complex with ct-DNA(Inset: Plots of $C_{ct\text{-}DNA}/(\varepsilon_a\text{-}\varepsilon_f)$ against $C_{ct\text{-}DNA}$ of **1** and **2**). The maximum absorption peaks of **1** were relatively flat at 332 and 389 nm where the bands exhibited hypochromism of 8.36% and 8.83% with slight red-shift [29-30] during the increase of the concentration of ct-DNA, indicating there was an intercalative mode between **1** and DNA [31], which was due to π→π* intercoupling between the π* empty orbit of **1** and the π orbital of ct-DNA base pairs after **1** inserted into ct-DNA [32,33]. The behavior of the interaction of **2** with ct-DNA was in a manner similar to **1**.

Figs.10-11

In order to determine and compare the binding abilities of **1** and **2** with ct-DNA, the binding constants K_b were calculated using Benesi-Hildebrand equation [34], the formula was as follows.

$$\frac{C_{ct\text{-}DNA}}{\varepsilon_a-\varepsilon_f}=\frac{C_{ct\text{-}DNA}}{\varepsilon_b-\varepsilon_f}+\frac{1}{K_b(\varepsilon_b-\varepsilon_f)} \qquad \text{Benesi-Hildebrand(5)}$$

Where $C_{ct\text{-}DNA}$ refers to the concentration of ct-DNA in base-pairs, K_b is apparent binding constant, ε_a is the apparent extinction coefficient of complexes, ε_b is the extinction coefficient of the complexes in the bound form and ε_f is the extinction coefficient of the complexes in the free form. K_b were obtained from the plots of $C_{ct\text{-}DNA}$ and $C_{ct\text{-}DNA}/(\varepsilon_a\text{-}\varepsilon_f)$ (as insets in Figs.10 and 11) and listed in Table 6. It was clearly seen from Table 6, the binding constant K_b of each complex with ct-DNA reached the order of magnitude of 10^7, and K_b(**1**)＞K_b(**2**), showing the binding ability of **1** with ct-DNA

was greater than that of **2**.

Table 6

3.5. DNA and BSA binding studies by microcalorimetry

Microcalorimetry was also used to study the biological activities between complexes and biological specimen [35-37]. Figs.12 and 13 displayed the thermogenic curves of each complex with ct-DNA and BSA at 28℃, respectively.

Figs.12-13

The maximum endothermic peaks of the interactions of **1** and **2** with ct-DNA appeared at 5.3 and 5.1 min and the reactions ended at 51.4 and 49.4 min, respectively, which were endothermic processes. The enthalpy changes(ΔH) obtained by integrating the peak area were listed in Table 7. As seen from Table 7, ΔH values were both beyond 2.0×10^4 kJ·mol^{-1} and ΔH(**1**-ct-DNA)＞ΔH(**2**-ct-DNA), showing the binding ability of **1** with ct-DNA was greater than that of **2**, consistent with the results of ct-DNA binding experiments. The maximum endothermic peaks of the interactions of **1** and **2** with BSA occurred at 5.2 and 6.5 min, and the reactions ended at 49.0 and 50.1 min, respectively, which were also endothermic processes, and ΔH(**1**-BSA) was almost four times than ΔH(**2**-BSA), indicating the binding ability of **1** with BSA was greater than that of **2**, corresponding to the results of BSA binding experiments. In order to calculate the ΔS and ΔG, the binding constants K_A from BSA binding experiments and K_b from ct-DNA binding experiments were substituted into the thermodynamic equations [38], respectively. The formulas were as follows.

$$\Delta G = -RT\ln K \quad (6)$$

$$\Delta S = (\Delta H - \Delta G)/T \quad (7)$$

Where ΔG refers to Gibbs function change, ΔS is the entropy change, ΔH is the enthalpy change, K_b is the apparent binding constant, T is the temperature in kelvin and

R is the gas constant. Δ*S* and Δ*G* were listed in Table 7. As seen from Table 7, Δ*G*<0, Δ*S*>0, and Δ*H*>0, illustrating the interactions of **1** and **2** with ct-DNA and BSA were spontaneous endothermic and entropy promoting processes.

Table 7

3.6. Antimicrobial activities

Fig.14 dispalyed the inhibition zones of **1** and **2** against *Escherichia coli*, *Staphylococcus aureus*, *Bacillus subtilis* and *Pseudomonas aeruginosa*. The average diameters (mm) of inhibition zones of DMF, gentamycin sulfate, **1** and **2** solutions were listed in Table 8. It is revealed that DMF (blank control) had a little effect on four kinds of bacteria, while gentamycin sulfate (control drug) had strong inhibition activities to them. Each complex exhibited obvious inhibition zones, the inhibition activity of **1** against *Pseudomonas aeruginosa* (16.36 mm) was strongest, followed by *Bacillus subtilis* (15.72 mm), but the inhibition activities of **1** against four kinds bacteria were not as great as that of gentamycin sulfate, while the inhibition activities of **2** against *Escherichia coli* (17.49 mm) and *Pseudomonas aeruginosa* (22.23 mm) were comparable to that of gentamycin sulfate at the concentration of 200 μg·mL^{-1}. When the concentrations of **1** and **2** were diluted to 50 μg·mL^{-1}, the average diameter of inhibition zones of **1** and **2** against four kinds of bacteria were similar to that of DMF (blank control), indicating the minimum inhibitory concentrations(MIC) of **1** and **2** against four kinds of bacteria were all 50 μg·mL^{-1}.

Fig.14

Table 8

4. Conclusions

Co(II) and Cr(III) complexes were prepared and X-ray single crystal diffraction indicated coordination atoms in two complexes exhibited octahedral geometry. The

thermal stabilities of **1** and **2** were studied by TG, showing **1** was more stable than **2**. BSA binding experiments indicated both of **1** and **2** quenched the intrinsic fluorescence of BSA through static processes. ct-DNA binding experiments displayed both of **1** and **2** bound to DNA efficiently by an intercalative mode. Microcalorimetry experiments illustrated the interactions of **1** and **2** with BSA and ct-DNA were both spontaneous endothermic and entropy promoting processes, and the interactions of **1** with BSA and ct-DNA were greater than that of **2**, corresponding to the results of BSA and ct-DNA binding experiments. The minimum inhibitory concentrations of each complex against four kinds of bacteria were all 50 $\mu g \cdot mL^{-1}$ and **2** exhibited strong inhibition activities against *Escherichia coli* and *Pseudomonas aeruginosa* at the concentration of 200 $\mu g \cdot mL^{-1}$, comparable to gentamycin sulfate.

Acknowledgments

The work was supported by the National Natural Science Foundation of China(Nos.21073139 and 21373158), Science and Technology on Combusion and Explosion Laboratory Foundation of Shaanxi (No.6142603010301), and Analytical Instrumentation Center of XUST.

Appendix A. Supplementary data

CCDC 1812120(**1**) and 1832625(**2**) contain the supplementary crystallographic data for this paper. These data can be obtained free of charge via http://www.ccdc.cam.ac.uk/conts/ retrieving.html, or from the Cambridge Crystallographic Data Centre, 12 Union Road, Cambridge CB2 1EZ, UK; fax: (+44)1223 336 033; or e-mail: deposit@ccdc.cam.ac.uk.

References

[1] V. Asati, N.K. Sahu, A. Rathore, S. Sahu, V. Kohli, Arabian J. Chem. 8 (2015) 495.

[2] J.G. Cui, L. Liu, D.D. Zhao, C.F. Gan, X. Huang, Q. Xiao, B.B. Qi, L. Yang, Y.M. Huang, Steroids 95 (2015) 32.

[3] N. Aggarwal, R. Kumar, C. Srivastva, P. Dureja, J. Khurana, J. Agric. Food Chem. 58 (2010) 3056.

[4] T. Sedaghat, M. Yousefi, G. Bruno, H.A. Rudbari, H. Motamedi, V. Nobakht, Polyhedron 79 (2014) 88.

[5] M.E. Bravo-Gómez, C. Campero-Peredo, D. Garcia-Conde, M.J. Mosqueira-Santillán, J. Serment, L. Ruiz-Azuara, Polyhedron 102 (2015) 530.

[6] X.P. Ye, T.F. Zhu, W.N. Wu, T.L. Ma, J. Xu, Z.P. Zhang, Y. Wang, L. Jia, Inorg. Chem. Commun. 47 (2014) 60.

[7] R. Yang, S.Y. He, W.T. Wu, Z.Y. Wen, Q.Z. Shi, D.Q. Wang, Acta Chim. Sin. 62 (2004) 2040.

[8] M.C. Rodriguez-Arguelles, R. Cao, A.M. Garcia-Deibe, C. Pelizzi, J. Sanmartin, F. Zani, Polyhedron 28 (2009) 2187.

[9] X.F. Han, H.X. Cai, L. Jia, W.N. Wu, X. Zhang, J. Xu, Z.P. Zhang, Y. Wang, J. Inorg. Chim. 31 (2015) 1453.

[10] W.J. Ni, H.Y. Qiong, H.J. Song, Y.X. Liu, Q.M. Wang, Scientia Sinica(Chimica) 47 (2017) 330.

[11] O. Derya, L. Serkan, K. Abdullah, I. Sinem, O. Yusuf, K. Zafer, Molecules 23 (2018) 1054.

[12] Z.Y. Yang, B. Song, C.Z. Zheng, S.W. Xu, Journal of Natuarl Science of Heilongjiang University 31 (2014) 367.

[13] R.S. Hunoor, B.R. Patil, D.S. Badiger, V.M. Chandrashekhar , I.S. Muchchandi, K.B. Gudasi, Appl. Organomet. Chem. 29 (2015) 101.

[14] J.H. Tang, H.Q. Wang, Y.Y. Wang, X.J. Jiang, H.L. Li, L. Jiang, S. Wang, Appl. Chem. Ind. 43 (2014) 31.

[15] A. Karakurt, M. Özalp, S. Işik, J.P. Stables, S. Dalkara, Bioorg. Med. Chem. 18 (2010) 2902.

[16] X.J. Zong, X.R. Liu, S.S. Zhao, Z.W. Yang, Chem. Res. & Appl. 30 (2018) 542.

[17] C.Y. Lin, K.F. Huang, Y.P. Yen, Spectrochim. Acta Part A. 115 (2013) 552.

[18] G.M. Sheldrick, Acta Crystallogr. 64 (2008) 112.

[19] J. Marmur, J. Mol. Biol. 3 (1961) 208.

[20] J.Z. Gu, D.Y. Lv, Z.Q. Gao, J.Z. Liu, W. Dou, Transition Met. Chem. 36 (2011) 53.

[21] A. Roth, J. Becher, C. Herrmann, H. Görls, G.B.M. Vaughan, M. Reiher, D. Klemm, W. Plass, Inorg. Chem. 45 (2006) 10066.

[22] H. Derakhshankhah, A.A. Saboury, A. Divsalar, H. Mansouri-Torshizi, Biophys. J. 100 (2011) 217.

[23] H.E. Kissinger, Anal. Chem. 29 (1957) 1702.

[24] T. Ozawa, Bull. Chem. Soc. Jpn. 38 (1965) 1881.

[25] G. H. Wu , C.H. Wang, Spectrosc. Spectral Anal. 25 (2005) 246.

[26] S. Soares, N. Mateus, V.D. Freitals, J. Agric. Food Chem. 55 (2007) 6726.

[27] N. Barbero, E. Barni, C. Barolo, P. Quagliotto, G. Viscardi, L. Napione, S. Pavan, F. Bussolino, Dyes Pigm. 80 (2009) 307.

[28] Y.H. Wu, X.L. Lan, N. Chen, L.Y. Liu, S.G. Xin, H.B. Zhang, Z. Yu, Chin. J. Anal. Lab. 33 (2014) 1365.

[29] C. Rajput, R. Rutkaite, L. Swanson, I. Haq, J.A. Thomas, Chem. Eur. J. 12 (2006) 4611.

[30] P.U. Maheswari, P. Mallayan, J. Inorg. Biochem. 98 (2004) 219.

[31] N. Chitrapriya, V. Mahalingam, M. Zeller, K. Natarajan, Inorg. Chim. Acta. 363 (2010) 3685.

[32] R. Natarajan, S. Sobha, Inorg. Chem. Commun. 17 (2012) 120.

[33] J. Eberhard, I. Stoll, R. Brockhinke, B. Neumann, H.G. Stammler, A. Riefer, E. Rauls, W.G. Schmidt, J. Mattay, Cryst. Eng. Commun. 15(2013) 4225.

[34] A.R. Wolfe, G.H. Shimer, T. Meehan, Biochemistry 26 (1987) 6392.

[35] M.N. Patel, B.S. Bhatt, P.A. Dosi, J. Therm. Anal. Calorim. 107 (2012) 55.

[36] L. Zhang, S.Y. Shao, H.Y. Wen, Life Science Instruments, 6 (2008) 28.

[37] A. Basu, G.S. Kumar, J. Chem. Thermodyn. 87 (2015) 1.

[38] D.P. Remeta, C.P. Mudd, R.L. Berger, K. Breslauer, Biochemistry 32(1993) 5064.

Scheme Captions

Scheme 1. Preparation routes of Co(II) complex(**1**) and Cr(III) complex(**2**).

Scheme 2. Two preparation routes of 2-acetylpyridine-6-bromo-2-naphthoyl acylhydrazone.

Scheme 3. The preparation mechanisms of two complexes.

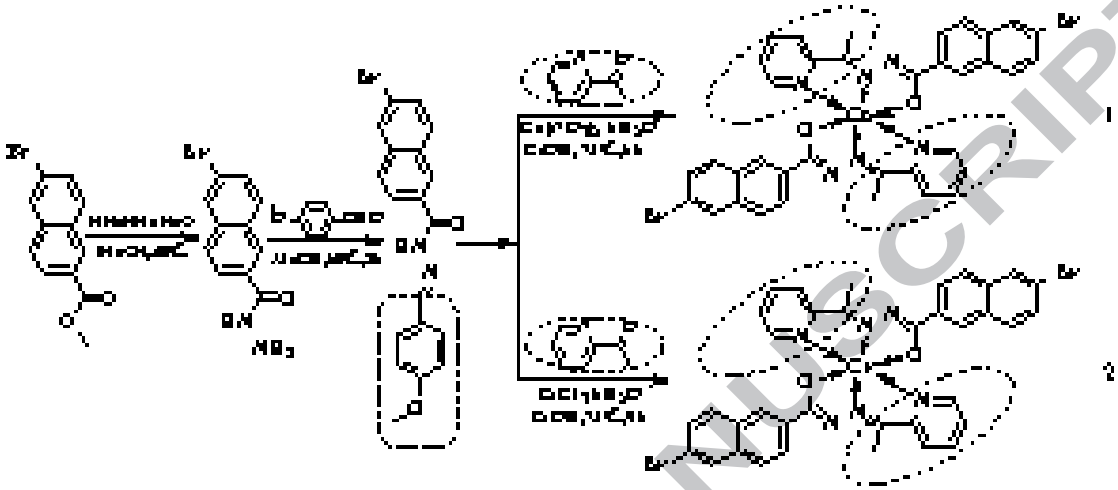

Scheme 1. Preparation routes of Co(II) complex(**1**) and Cr(III) complex(**2**).

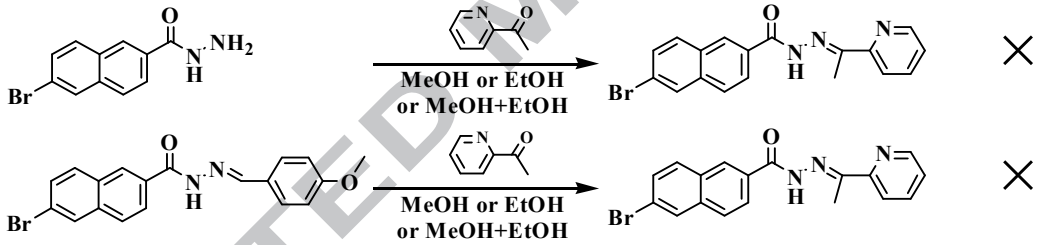

Scheme 2. Two preparation routes of 2-acetylpyridine-6-bromo-2-naphthoyl acylhydrazone.

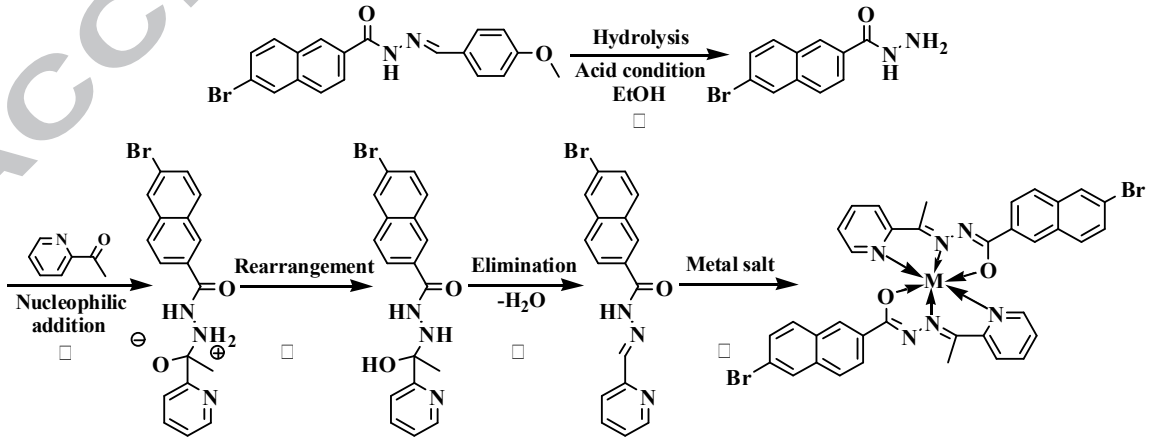

Scheme 3. The preparation mechanisms of two complexes.

Table Captions

Table 1 Crystallographic data of **1** and **2**.

Table 2 Selected bond length(Å) and bond angle(°) of **1** and **2**.

Table 3 Kinetic parameters of thermal decomposition of **1** and **2**.

Table 4 Dynamic fluorescence quenching parameters of the interactions of **1** and **2** with BSA.

Table 5 Static fluorescence quenching parameters of the interactions of **1** and **2** with BSA.

Table 6 The binding parameters of **1** and **2** with ct-DNA.

Table 7 Thermodynamic parameters of the interactions of **1** and **2** with ct-DNA and BSA.

Table 8 The average diameters (mm) of inhibition zones of DMF, gentamycin sulfate, **1** and **2** solutions.

Table 1 Crystallographic data of **1** and **2**.

Complex	**1**	**2**
Chemical formula	$C_{36}H_{26}Br_2CoN_7O_5$	$C_{36}H_{26}Br_2CrN_6O_2$

Formula weight	857.46	788.46
CCDC	1812120	1832625
Crystal system	Monoclinic	Triclinic
Space group	$P2_1/n$	P-1
a(Å)	13.680(5)	11.4942(19)
b(Å)	11.973(4)	12.459(2)
c(Å)	23.323(8)	15.401(3)
α(°)	90.000	72.181(3)
β(°)	103.775(8)	74.300(3)
γ(°)	90.000	75.692(3)
V(Å^3)	3710(2)	1988.6(6)
Z	4	2
D_{calc}(g/cm^3)	1.614	1.370
F(000)	1816	824
θ Range	1.58-26.10	1.41-25.10
Goodness-of-fit on F^2	0.863	1.097
Limiting indices	-16≤h≤16 -13≤k≤14 -19≤l≤28	-11≤h≤13 -14≤k≤14 -18≤l≤18
Final R indices[I>2sigma(I)]	R_1 = 0.0701, wR_2 = 0.1469	R_1 = 0.1396, wR_2 = 0.3989
R indices (all data)	R_1 = 0.3123, wR_2 = 0.2684	R_1 = 0.2250, wR_2 = 0.4746

Table 2 Selected bond length(Å) and bond angle(°) of **1** and **2**.

Complex	Bond	Length/Å	Bond	Angle/(°)
1	Co(1)-N(2)	1.849(9)	N(2)-Co(1)-N(5)	175.3(5)
	Co(1)-N(5)	1.865(9)	N(3)-Co(1)-O(1)	164.3(4)
	Co(1)-O(2)	1.902(8)	N(6)-Co(1)-O(2)	164.2(4)
	Co(1)-N(3)	1.921(10)	N(2)-Co(1)-O(2)	93.3(4)
	Co(1)-N(6)	1.953(11)	N(2)-Co(1)-N(3)	81.6(5)
	Co(1)-O(1)	1.907(7)	N(3)-Co(1)-N(6)	91.9(4)
	N(1)-C(11)	1.313(13)	N(5)-Co(1)-N(3)	97.9(4)
	C(11)-O(1)	1.330(13)	O(1)-Co(1)-O(2)	90.5(3)
	C(12)-N(2)	1.277(13)	N(4)-N(5)-Co(1)	116.0(8)
2	Cr(1)-N(2)	1.956(9)	N(2)-Cr(1)-N(5)	172.8(4)
	Cr(1)-N(5)	1.935(9)	N(3)-Cr(1)-O(1)	155.9(4)
	Cr(1)-O(2)	1.961(8)	N(6)-Cr(1)-O(2)	156.6(3)
	Cr(1)-N(3)	2.065(10)	N(2)-Cr (1)-O(2)	107.3(4)
	Cr(1)-N(6)	2.068(9)	N(2)-Cr(1)-N(3)	78.1(4)
	Cr(1)-O(1)	1.954(8)	N(3)-Cr(1)-N(6)	92.3(4)
	N(1)-C(11)	1.317(15)	N(5)-Cr(1)-N(3)	97.1(4)
	C(11)-O(1)	1.319(12)	O(1)-Cr(1)-O(2)	94.1(4)
	C(12)-N(2)	1.288(15)	N(4)-N(5)-Cr(1)	118.8(7)

Table 3 Kinetic parameters of thermal decomposition of **1** and **2**.

Complex	β/℃·min^{-1}	T_P/℃	Kissinger			Ozawa	
			E_a/kJ·mol^{-1}	lg$A$	r	E_a/kJ·mol^{-1}	r

	5	281.73					
1	10	285.84	480.6	43.43	-0.994	465.8	-0.994
	15	287.36					
	5	277.84					
2	10	283.34	190.0	15.85	-0.987	189.5	-0.981
	15	291.69					

Table 4 Dynamic fluorescence quenching parameters of the interactions of **1** and **2** with BSA.

Complex	Stern-Volmer Fitting Equations	K_{sv}/L·mol^{-1}	K_q/L·mol^{-1}·s^{-1}	R^2
1	F_0/F=2.45×10^5Q +1.011	2.45×10^5	2.45×10^{13}	0.989
2	F_0/F=3.04×10^5Q +1.023	3.04×10^5	3.04×10^{13}	0.987

Table 5 Static fluorescence quenching parameters of the interactions of **1** and **2** with BSA.

Complex	Lineweaver-Burk Fitting Equations	K_A/L·mol^{-1}	n	R^2
1	lg[(F_0-F)/F]=0.814lg[Q]+4.25	1.79×10^4	0.814	0.988
2	lg[(F_0-F)/F]=0.779lg[Q]+4.16	1.43×10^4	0.779	0.997

Table 6 The binding parameters of **1** and **2** with ct-DNA.

Complex	Fitting Equations	K_b/L·mol^{-1}	R^2
1	$C_{ct\text{-}DNA}$/(ε_a-ε_f)=2.69×10^{-5} $C_{ct\text{-}DNA}$ +1.62×10^{-12}	1.67×10^7	0.999
2	$C_{ct\text{-}DNA}$/(ε_a-ε_f)=6.19×10^{-5} $C_{ct\text{-}DNA}$ +4.95×10^{-12}	1.25×10^7	0.999

Table 7 Thermodynamic parameters of the interactions of **1** and **2** with ct-DNA and BSA.

System	ΔG (kJ·mol^{-1})	ΔS (kJ·mol^{-1}·K^{-1})	ΔH (kJ·mol^{-1})	Start time (min)	End time (min)	Action time (min)
1+ct-DNA	-41.62	85.47	2.57×10^4	3.6	51.4	47.5
2+ct-DNA	-40.92	68.54	2.06×10^4	3.7	49.4	45.7
1+BSA	-24.50	147.18	4.43×10^4	3.8	49.0	45.2
2+BSA	-23.99	32.27	1.12×10^4	4.3	50.1	45.8

Table 8 The average diameters (mm) of inhibition zones of DMF, gentamycin sulfate, **1** and **2** solutions.

Compound	Concentration ($\mu g \cdot mL^{-1}$)	Inhibition zone diameter (mm)			
		Escherichia coli	*Staphylococcus aureus*	*Bacillus subtilis*	*Pseudomonas aeruginosa*
DMF	-	9.54	9.19	9.50	9.41
Gentamycin sulfate	200	17.86	16.36	16.24	22.28
1	200	13.21	13.01	15.72	16.36
2	200	17.49	11.94	13.83	22.23
1	100	12.17	10.23	12.53	12.88
2	100	11.00	10.41	11.18	11.44
1	50	10.38	9.56	9.96	10.34
2	50	9.89	9.47	10.18	10.19

Figure Captions

Fig.1. Molecular structure of **1**.

Fig.2. Crystal packing structure of **1**.

Fig.3. Molecular structure of **2**.

Fig.4. Crystal packing structure of **2**.

Fig.5. TG-DTG curves of **1**.

Fig.6. TG-DTG curves of **2**.

Fig.7. Fluorescence emission spectra of the interaction of **1** with BSA(Inset: Plot of F_0/F against Q of **1**).

Fig.8. Fluorescence emission spectra of the interaction of **2** with BSA(Inset: Plot of F_0/F against Q of **2**).

Fig.9. Plots of lg[$(F_0$-$F)/F$] against lg[Q] of **1** and **2**.

Fig.10. UV-vis spectra of the interaction of **1** with ct-DNA(Inset: Plot of $C_{\text{ct-DNA}}/(\varepsilon_a$-$\varepsilon_f)$ against $C_{\text{ct-DNA}}$ of **1**).

Fig.11. UV-vis spectra of the interaction of **2** with ct-DNA(Inset: Plot of $C_{\text{ct-DNA}}/(\varepsilon_a$-$\varepsilon_f)$ against $C_{\text{ct-DNA}}$ of **2**).

Fig.12. Thermogenic curves of the interactions between **1** and **2** with ct-DNA.

Fig.13. Thermogenic curves of the interactions between **1** and **2** with BSA.

Fig.14. (a) The inhibition zones of **1** against four kinds of bacteria. (b) The inhibition zones of **2** against four kinds of bacteria. (A, B, C and D represent *Escherichia coli*, *Staphylococcus aureus*, *Bacillus subtilis* and *Pseudomonas aeruginosa*, respectively. 1, 2 and 3 represent 200, 100 and 50 μg ·mL^{-1}, respectively.).

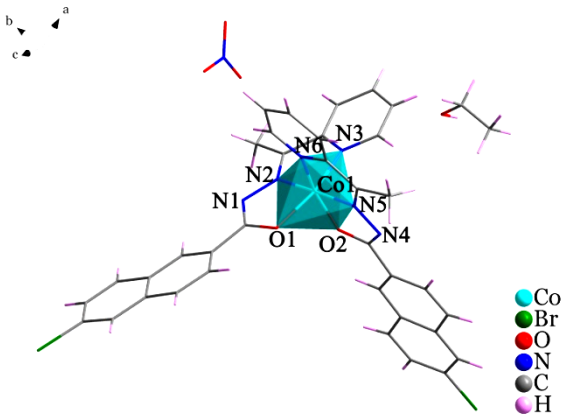

Fig.1. Molecular structure of **1**.

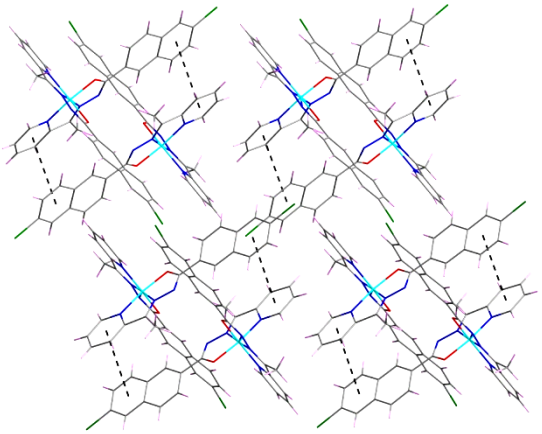

Fig.2. Crystal packing structure of **1**.

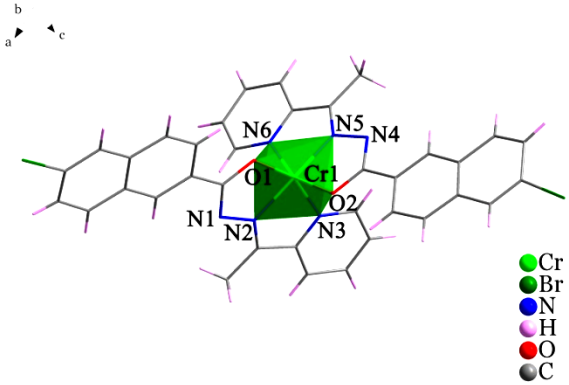

Fig.3. Molecular structure of **2**.

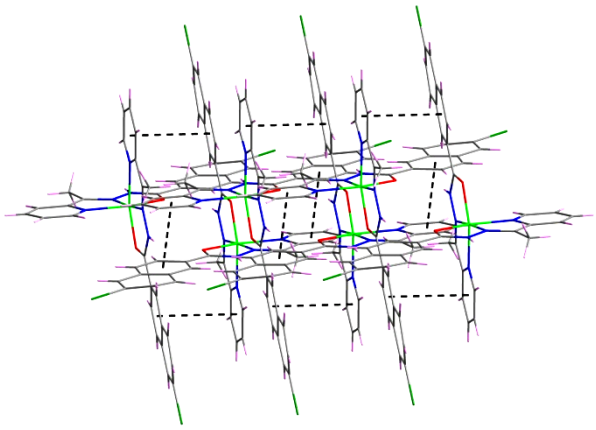

Fig.4. Crystal packing structure of **2**.

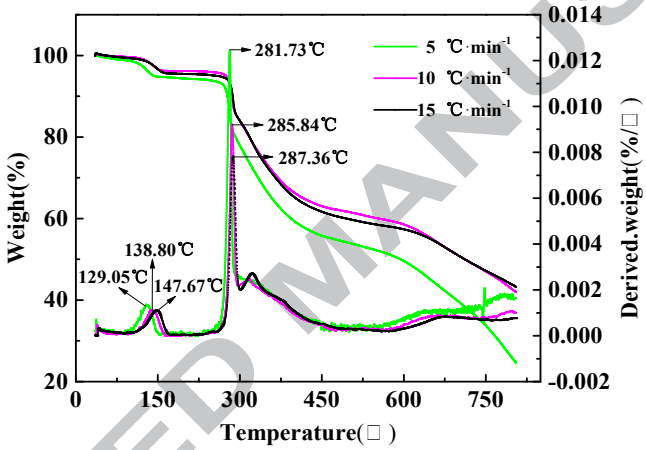

Fig.5. TG-DTG curves of **1**.

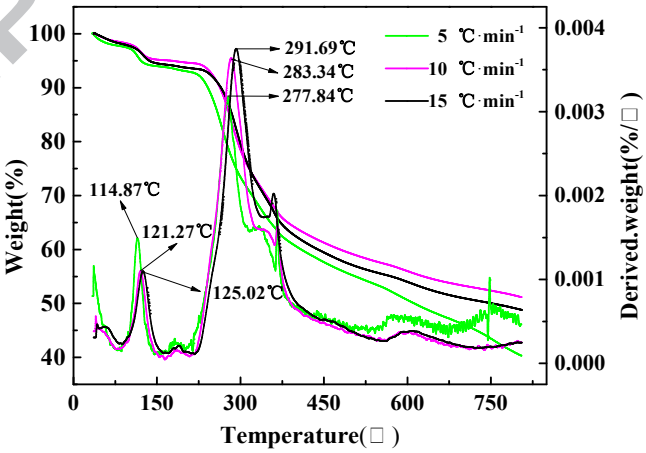

Fig.6. TG-DTG curves of **2**.

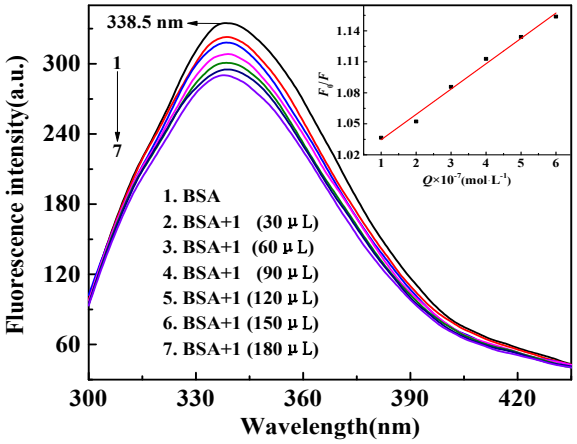

Fig.7. Fluorescence emission spectra of the interaction of **1** with BSA(Inset: Plot of F_0/F against Q of **1**).

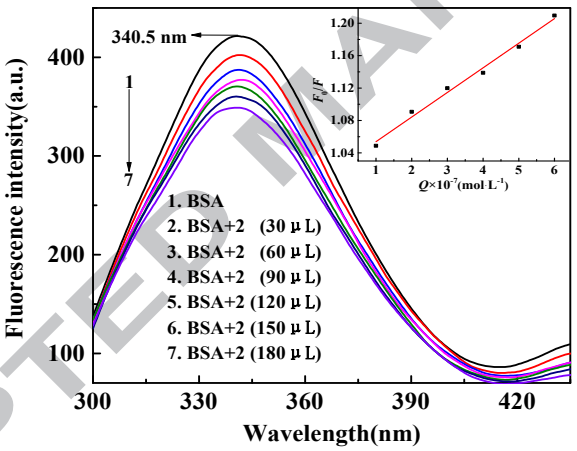

Fig.8. Fluorescence emission spectra of the interaction of **2** with BSA(Inset: Plot of F_0/F against Q of **2**).

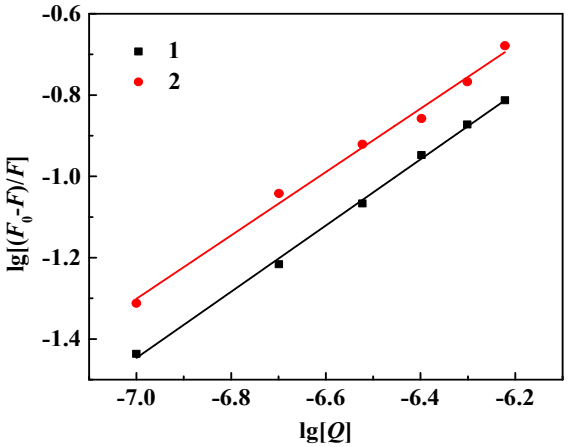

Fig.9. Plots of lg[$(F_0$-$F)/F$] against lg[Q] of **1** and **2**.

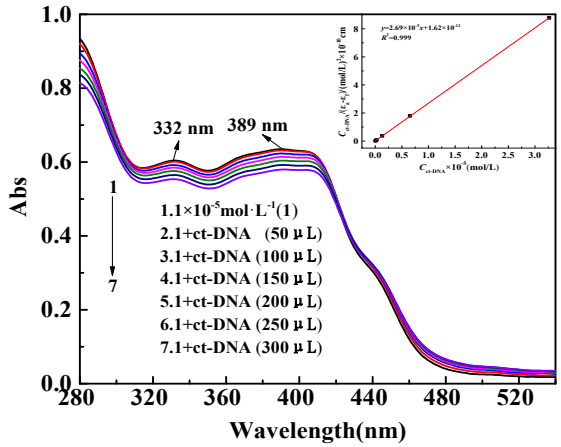

Fig.10. UV-vis spectra of the interaction of **1** with ct-DNA

(Inset: Plot of $C_{ct\text{-}DNA}/(\varepsilon_a\text{-}\varepsilon_f)$ against $C_{ct\text{-}DNA}$ of **1**).

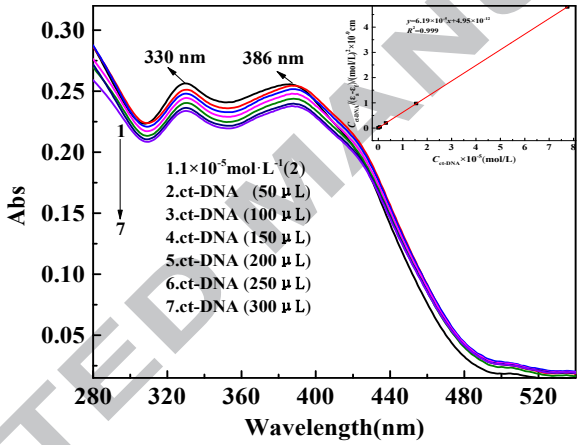

Fig.11. UV-vis spectra of the interaction of **2** with ct-DNA

(Inset: Plot of $C_{ct\text{-}DNA}/(\varepsilon_a\text{-}\varepsilon_f)$ against $C_{ct\text{-}DNA}$ of **2**).

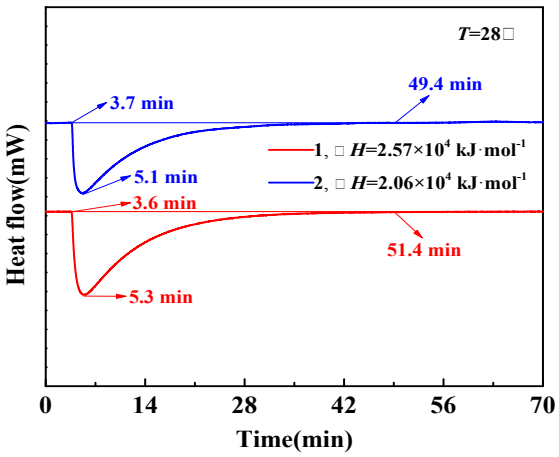

Fig.12. Thermogenic curves of the interactions between **1** and **2** with ct-DNA.

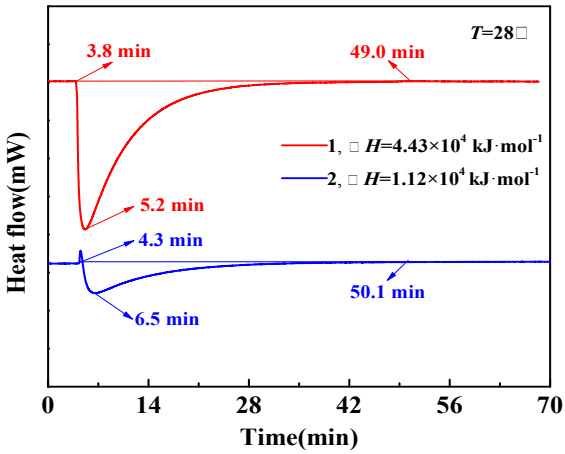

Fig.13. Thermogenic curves of the interactions between **1** and **2** with BSA.

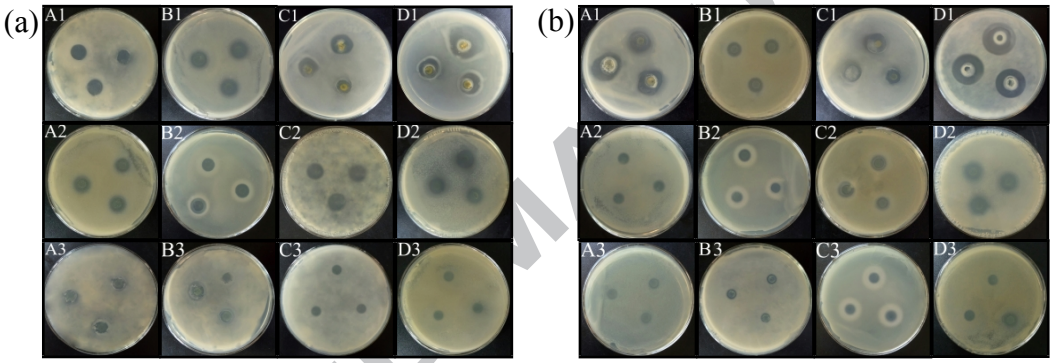

Fig.14. (a) The inhibition zones of **1** against four kinds of bacteria. (b) The inhibition zones of **2** against four kinds of bacteria. (A, B, C and D represent *Escherichia coli*, *Staphylococcus aureus*, *Bacillus subtilis* and *Pseudomonas aeruginosa*, respectively. 1, 2 and 3 represent 200, 100 and 50 μg·mL^{-1}, respectively.).

Graphical Abstract

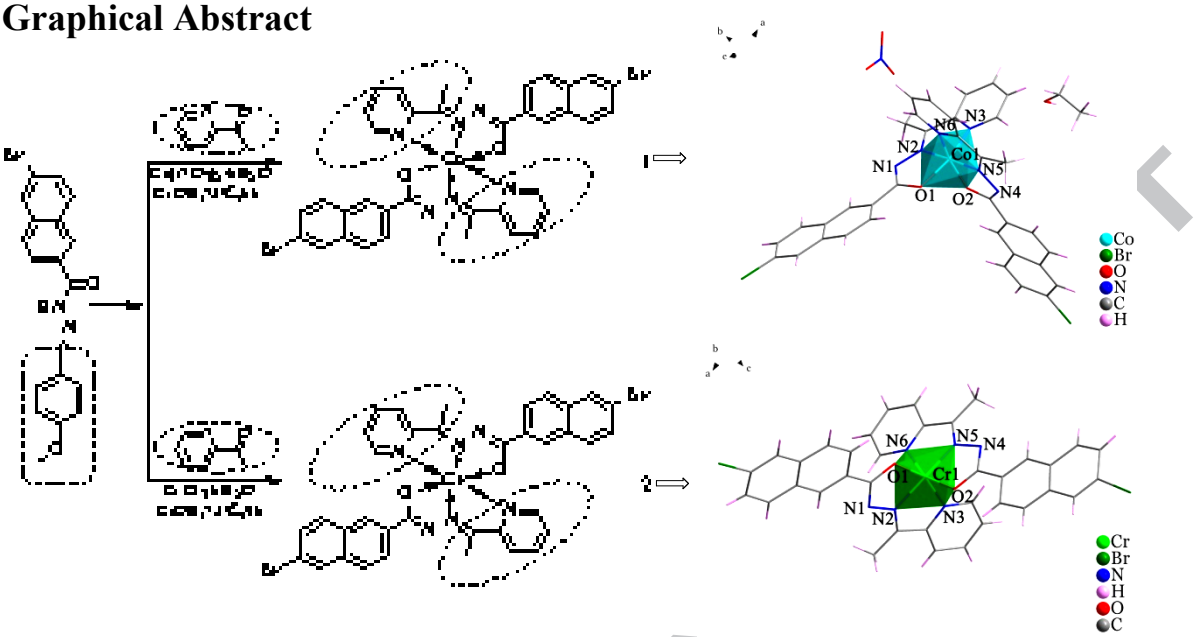

Two novel Co(II) and Cr(III) complexes were prepared, and the constitutes and strctures of two complexes were characterizated by elemental analysis, melting point test and X-ray single crystal diffraction technique. Furthermore, the thermal stabilities of Co(II) and Cr(III) complexes were discussed and the interactions of Co(II) and Cr(III) complexes with BSA and ct-DNA were studied by spectrometry and microcalorimetry. The inhibition activities of Co(II) and Cr(III) complexes against four kinds of bacteria were investigated and compared with that of gentamycin sulfate.